ISSN 2616-5767 Vol.9, Issue 1: 13-23, DOI: 10.25236/AJETS.2026.090102

Screen-Printed Ink Protrusion Defect Detection Method for Mobile Phone Cover Glass

Kaijie Chen[1,a], Xiangqian Peng[1,b,*], Yingjie Xiao[1,c]

[1]School of Mechanical and Electrical Engineering, Hunan University of Science and Technology, Xiangtan, China
[a]kaijiec29@gmail.com, [b]2939337692@qq.com, [c]3222419925@qq.com
[*]Corresponding author

Abstract: *During the screen-printing process of mobile phone cover glass, factors such as ink accumulation, non-uniform squeegee scraping, and environmental vibration can easily induce tiny ink-protrusion defects along the edge region. These defects are characterized by small size and weak grayscale contrast, and are often accompanied by glass specular reflections and screen-printing texture interference, posing significant challenges for online inspection. To address this problem, this paper proposes a screen-printed ink protrusion defect detection method based on image enhancement and row-wise scanning statistics. First, bilateral filtering is applied to enhance the screen-printed edges, suppressing noise while preserving edge structures and improving the discriminability of low-contrast defects. Next, the bottom contour is extracted using Canny edge detection, and a bottom reference line is selected via Hough line fitting; this line is then used to partition the inspection region and establish row-scanning baselines. Finally, leveraging the local grayscale anomaly of protrusions along the row direction, a row-wise pixel accumulation and ratio-thresholding strategy is designed: edge feature values are computed for each row, abnormal rows whose responses rise above a certain proportion of the row-wise mean are selected, and a consecutive-row triggering mechanism is introduced to achieve stable identification and localization of protrusion defects. Experimental results demonstrate that the proposed method can effectively detect screen-printed ink protrusion defects and exhibits good robustness under complex conditions involving reflections and texture interference, satisfying the requirements of practical production lines for online inspection of screen-printing defects.*

Keywords: *mobile phone cover glass; screen printing; protruding defect; defect detection*

1. Introduction

With the rapid development of the smartphone industry [1], product appearance quality has become one of the key factors influencing market competitiveness. As a critical component of a smartphone's exterior, the cover glass undergoes multiple cycles of ink printing and curing during the screen-printing process to form functional and decorative patterns such as characters, marks, and window coatings [2]. A typical screen-printing workflow is shown in Figure. 1. In practical manufacturing, the process is easily affected by factors including fluctuations in ink viscosity, unstable squeegee pressure, insufficient surface cleanliness of the glass, and equipment vibration. These factors may lead to local ink accumulation, scraping residues, or slight ink overflow near the edge region, thereby producing ink-protrusion defects. Although such defects are usually small in size, they can significantly degrade appearance uniformity and perceived quality. If not detected and removed in time during production, they may reduce yield, increase rework costs, and even cause appearance-related customer complaints at the end-use stage. Conventional manual inspection mainly relies on visual judgment, and suffers from low efficiency, fatigue-related errors, poor stability, and high miss rates, making it difficult to meet the requirements of modern production lines for high-precision, high-consistency, and high-throughput online inspection. Therefore, developing a stable and reliable machine-vision-based automated inspection method for screen-printed defects on mobile phone cover glass is of important engineering value and practical significance.

Considering recent research progress and production-line deployment practices, automated inspection technologies for screen-printing defects on mobile phone cover glass can generally be categorized into two main paradigms: traditional machine-vision-based methods and deep-learning-based methods.

ISSN 2616-5767 Vol.9, Issue 1: 13-23, DOI: 10.25236/AJETS.2026.090102

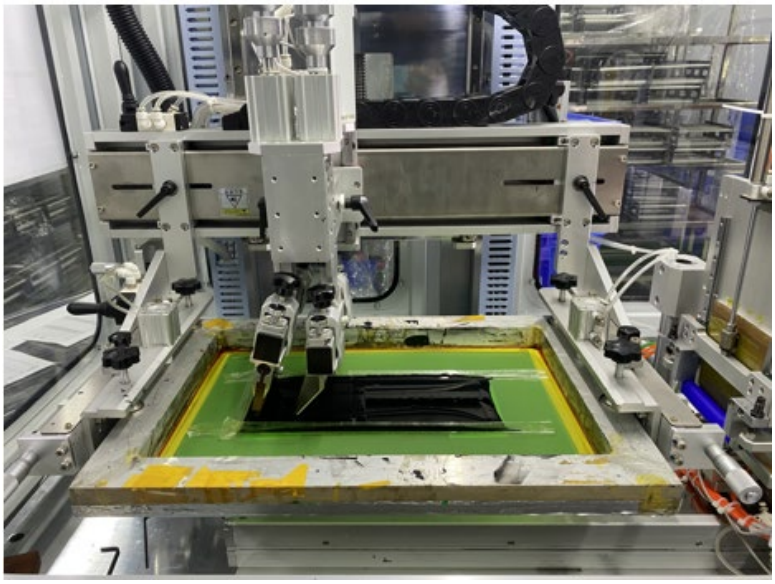

Figure 1: Screen-Printing Process Flow.

Traditional approaches are typically built upon image preprocessing and geometric alignment. They localize defect regions through operations such as image differencing, threshold segmentation, morphological processing, and feature extraction, and then perform recognition using classifiers. Liu et al.[3] combined a line-intercept thresholding strategy with particle swarm optimization to address insufficient detection accuracy in mobile phone screen defect inspection. Zhang Caixia et al. [4] integrated Otsu thresholding and K-means clustering under backlight illumination to effectively discriminate defects such as watermarks, scratches, and pinholes on glass surfaces. Cai Nian et al.[5] developed a feature-engineering scheme for quality inspection of glass-packaged insulating terminals, combining shape priors and multi-dimensional image features with a gradient boosting decision tree to achieve finer classification and improved performance. Chen Ning et al.[6] targeted curved glass scenarios and integrated shape matching, connected-component analysis, and frequency-domain enhancement to realize defect identification and dimensional measurement. Although traditional machine-vision methods offer advantages such as simplicity, interpretability, and low computational cost, they often rely on manually designed features and threshold rules in practice, making them sensitive to illumination variations, noise levels, batch-to-batch differences, and complex backgrounds. Moreover, inappropriate handling of feature selection, dimensionality reduction, or classifier generalization may lead to increased false positives and degraded detection stability.

With the development of deep learning, representative object detection frameworks such as Faster R-CNN [7], YOLO [8], and SSD [9] have demonstrated stronger feature representation capabilities and robustness across a wide range of industrial vision tasks, accelerating the adoption of CNN-based approaches in defect inspection. Yuan et al. [10] developed a defect inspection device for mobile phone cover glass based on backlight line-scan imaging. By improving the imaging signal-to-noise ratio and incorporating an enhanced segmentation strategy, they achieved defect extraction and measurement, and their experimental results indicated that the method could attain high detection accuracy. Lv et al. [11] further combined Faster R-CNN with a generative adversarial network to enhance defect feature representation and extraction, and experiments likewise verified the effectiveness of the proposed approach. Overall, these studies highlight the advantages of deep learning in glass defect inspection. However, in real production-line environments, performance is still constrained by multiple uncertainties, such as shifts in imaging conditions, changes in data distribution, the high cost of annotating tiny defects, and stringent requirements on inference speed and operational stability, all of which can affect model generalization and deployability.

For defects such as raised areas in screen-printed ink—characterized by extremely small dimensions, low contrast, and proximity to regular edges (as shown in Figure 2)—automated detection poses particularly severe technical challenges. On one hand, such defects occupy an extremely low proportion of pixels in images and closely resemble screen printing edge textures in both grayscale distribution and local morphology, making them prone to being overwhelmed by strong edge structures during feature extraction. On the other hand, subsampling operations—commonly employed to obtain larger receptive fields—further weaken fine-grained protrusion features, making them difficult to effectively preserve in

ISSN 2616-5767 Vol.9, Issue 1: 13-23, DOI: 10.25236/AJETS.2026.090102

feature maps. Due to the combined effects of these factors, both traditional machine vision methods based on manually designed features and data-driven deep learning models struggle to achieve stable and reliable detection of such defects under actual production conditions.

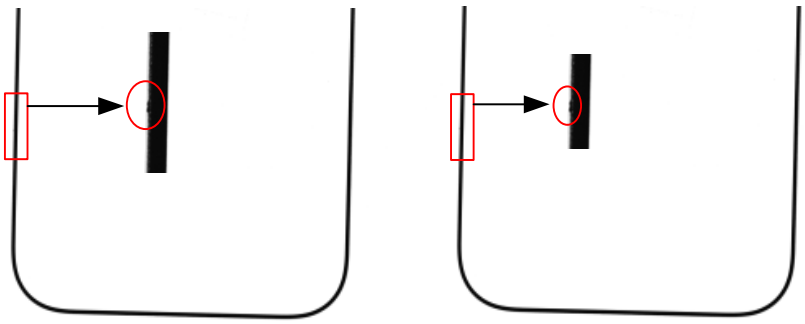

Figure 2: Ink Protrusion Defect.

To address the above issues, this paper proposes an ink protrusion defect detection method tailored to the screen-printing scenario of mobile phone cover glass, following an overall pipeline of "image enhancement–geometric baseline construction–row-wise statistical decision." First, the original image is enhanced (e.g., edge-preserving denoising and contrast enhancement) to improve the separability of low-contrast protrusion features. Next, the image is segmented based on the stable geometric structure of the screen-printed edges, and row-scanning baselines are constructed (three baselines/three baseline types can be defined to constrain the scanning start positions and statistical regions). Finally, leveraging the grayscale distribution characteristics of the screen-printed edges along image rows, a row-wise scanning statistical algorithm is designed to achieve stable identification and localization of protrusion defects through edge-response accumulation, abnormal-row selection, and a continuity constraint. The main contributions of this work are as follows:

(1) A unified detection framework integrating enhancement, baseline construction, and row-wise scanning statistics is developed, enabling stable highlighting and detection of tiny ink protrusions under low-contrast and complex-background conditions.

(2) A boundary-protrusion decision strategy based on row-wise pixel accumulation and statistical thresholding is proposed, together with a continuity constraint to suppress isolated noise interference, featuring low computational cost, simple implementation, and easy deployment in industrial environments.

2. Defect Detection Method

Based on a detailed analysis of the formation mechanisms of screen-printed ink protrusion defects and their image-level characteristics, this section develops a defect detection method following the overall pipeline of "enhancement–segmentation–row-wise scanning statistics." First, bilateral filtering is applied to the screen-printed edge region for edge-preserving enhancement, which suppresses noise and speckle artifacts while improving the separability of low-contrast protrusion defects, thereby providing a more reliable basis for subsequent feature extraction. Next, given that protrusion defects are mainly distributed along the outer screen-printed edge, a reference edge line is extracted via Hough line fitting and used to partition the image into four sub-regions (left, right, upper, and lower) to define the inspection areas. Subsequently, a row-wise scanning statistical algorithm tailored to the screen-printed edge is designed, in which row-wise pixel accumulation, threshold-based decision making, and a consecutive-row constraint are jointly employed to achieve stable identification and precise localization of ink protrusion defects. Considering the resolution and accuracy requirements of on-line inspection, full cover-glass imaging is performed using two industrial cameras that separately capture the upper and lower fields of view. As the detection procedure and parameter settings are consistent for both views, this study focuses on the lower-half images for method description and experimental validation. The above steps constitute the complete detection pipeline of the proposed approach, as illustrated in Figure. 3.

ISSN 2616-5767 Vol.9, Issue 1: 13-23, DOI: 10.25236/AJETS.2026.090102

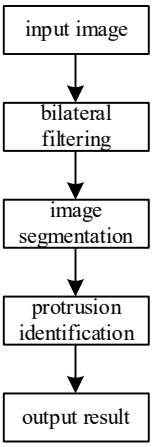

Figure 3: Detection Flowchart.

2.1 Image Enhancement

In screen-printed mobile phone cover-glass images, ink-protrusion defects are typically characterized by extremely small size and low contrast. To enable more stable edge-feature extraction in the subsequent row-wise scanning statistical analysis, bilateral filtering is applied to the original images as an enhancement pre-processing step. Bilateral filtering suppresses random noise while effectively preserving edge structures, thereby providing a more reliable input for downstream feature extraction and statistical decision-making.

Bilateral filtering [12] is a typical nonlinear edge-preserving smoothing technique. Its core idea is to perform low-noise, edge-preserving filtering by jointly considering a spatial-distance weight and an intensity-similarity (grayscale) weight between pixels. The filtered output can be expressed as:

$$I^{BF}(p)=\frac{1}{W_p}\sum_{q\in\Omega}I(q)f_s(\|p-q\|)f_r(|I(p)-I(q)|) \tag{1}$$

Where Ω denotes the neighborhood window centered at pixel p; $f_s(\cdot)$ is the spatial-domain weighting function (typically a Gaussian kernel); $f_r(\cdot)$ is the range (intensity) weighting function (also commonly modeled by a Gaussian function); and W_p is the normalization factor used to ensure proper weighting of the filter response, defined as:

$$W_p=\sum_{q\in\Omega}f_s(\|p-q\|)f_r(|I(p)-I(q)|) \tag{2}$$

The spatial kernel describes that pixels farther away from the current pixel have a weaker influence. It is typically modeled by a Gaussian function:

$$f_s(\|p-q\|)=\exp\left(-\frac{\|p-q\|^2}{2\sigma_s^2}\right) \tag{3}$$

where σ_s controls the spatial smoothing range; a larger σ_s leads to a wider spatial neighborhood influence.

The range (intensity) kernel indicates that a larger gray-level difference corresponds to a lower similarity. It is also commonly modeled by a Gaussian function:

$$f_r(|I(p)-I(q)|)=\exp\left(-\frac{(I(p)-I(q))^2}{2\sigma_r^2}\right) \tag{4}$$

Here, σ_r controls the sensitivity to intensity similarity. When a pronounced intensity discontinuity occurs at an edge, the gray-level difference between pixels causes the range weight to decay rapidly, thereby suppressing smoothing across the edge and preventing edge blurring.

To verify the effectiveness of bilateral filtering in noise suppression and edge preservation, a

ISSN 2616-5767 Vol.9, Issue 1: 13-23, DOI: 10.25236/AJETS.2026.090102

comparative experiment was conducted using screen-printed edge samples acquired by an industrial camera, and the results are shown in Fig. 4. As can be observed in Fig. 4(a), the original image exhibits noticeable noise and intensity fluctuations near the screen-printed edge, where tiny protrusion features are mixed with background edge textures and the local contrast is relatively weak. After bilateral-filter enhancement (Fig. 4(b)), the background noise is substantially suppressed and the screen-printed edge contour becomes more continuous and smoother, while fine edge details are preserved without obvious blurring or fragmentation. Moreover, the grayscale contrast in the protrusion region is further enhanced, making it more likely to produce stable abnormal responses during the subsequent row-wise scanning statistical analysis.

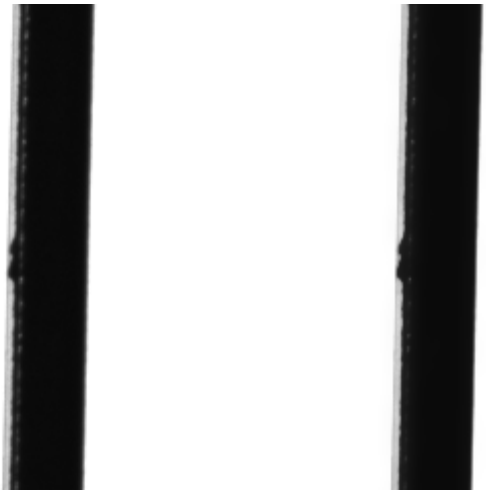

(a) Original image *(b) Bilateral-filtered image*

Figure 4: Enhancement Comparison Results.

2.2 Image Segmentation

In automated vision inspection of screen-printed cover glass, different defect types exhibit distinct spatial distributions in the image. In particular, ink-protrusion defects are mainly generated and concentrated along the outer screen-printed edge. Therefore, an outside-to-inside row-scanning strategy is adopted to ensure that the scanning starts from the high-incidence edge region and progresses inward. To enable consistent scan initialization and stable statistical regions for subsequent row-wise analysis, a reliable spatial partition baseline must be established in advance. Given that the bottom edge of the screen-printed cover glass is continuous, easy to extract, and geometrically stable, this study uses the bottom edge as the geometric reference: based on the extracted edge map, the bottom edge is fitted using the Hough line transform [13], and candidate lines are further screened according to geometric parameters such as slope and intercept. The reference line that best matches the bottom-edge contour is then selected for image segmentation and region constraint.

2.2.1 Edge Detection

In industrial vision applications, the quality of edge extraction directly affects the accuracy of subsequent line fitting, region segmentation, and geometric measurement. Traditional edge operators such as Prewitt and Roberts [14] are computationally efficient due to their simple structures; however, they are limited in gradient-direction modeling and are sensitive to noise, which often leads to edge fragmentation or localization bias. The Sobel operator [15] improves noise robustness by incorporating smoothing weights, but its response to complex textures and weak edges remains limited. Second-order operators, including the Laplacian and the Laplacian of Gaussian (LoG), can enhance weak edges; nevertheless, second-order derivatives are still noise-sensitive and may introduce spurious edges.

In contrast, the Canny algorithm [16] employs a multi-stage pipeline—Gaussian smoothing, gradient computation, non-maximum suppression, and double-threshold hysteresis linking—to produce edges that are more continuous and more accurately localized under texture complexity and noise interference. Its gradient estimation integrates multi-directional responses, making it more suitable for curved boundaries, weak edges, and low-contrast regions. Moreover, Gaussian filtering reduces noise effects [17], while the double-threshold strategy effectively connects broken edges, thereby balancing edge continuity and accuracy. Therefore, this study adopts the Canny algorithm to extract pixel-level edges in the screen-

ISSN 2616-5767 Vol.9, Issue 1: 13-23, DOI: 10.25236/AJETS.2026.090102

printing region, and its main steps are as follows:

(1) A Gaussian filter is applied to smooth the original image in order to suppress noise and reduce spurious edges caused by abrupt gray-level variations. The smoothing operation is given in equation :

$$G(x,y)=\frac{1}{\sqrt{2\pi\sigma^2}}e^{-\left(x^2+y^2\right)/2\sigma^2} \tag{5}$$

(2) The smoothed image is convolved with derivative kernels to obtain the gradient components in the horizontal and vertical directions. The gradient magnitude A is then computed using equation (6), and the gradient orientation is calculated using equation (7).

$$\mathrm{A}=\sqrt{G_x^{\,2}+G_y^{\,2}} \tag{6}$$

$$\theta=\arctan\left(G_y/G_x\right) \tag{7}$$

(3) Non-maximum suppression is applied to eliminate redundant edge responses. By scanning the gradient magnitude map, only the pixels corresponding to local maxima along the gradient direction are retained.

(4) A double-threshold scheme is used to classify pixels: those with gradient magnitudes above the high threshold are labeled as strong edges, those below the low threshold are regarded as non-edge pixels, and those between the two thresholds are treated as weak (candidate) edges.

(5) Hysteresis edge tracking is performed for the weak (candidate) edge pixels. A weak edge is retained as a valid edge if there exists a connected strong edge within its 8-neighborhood; otherwise, it is suppressed as noise.

As shown in Figure 5, Canny edge detection not only delineates the overall outer contour more completely but also preserves potential abnormal structural cues near the boundary, thereby providing a reliable input for subsequent line fitting and region partitioning.

Figure 5: Canny Edge Detection Results.

2.2.2 Line Fitting and Region Partitioning

After extracting the edge contours, line fitting is further performed to establish a geometric reference for subsequent region partitioning. In this study, the bottom edge is fitted using the Hough line transform, which detects straight lines in a parametric space and yields a globally consistent reference line with strong robustness to noise. To improve segmentation efficiency, only one dominant line is fitted in the bottom region to achieve an initial global partition of the image. Subsequently, the upper region is evenly bisected according to its geometric symmetry to obtain two sub-regions (left and right). This “single fitting + simplified partitioning” strategy avoids the computational overhead of repeated fitting while

ISSN 2616-5767 Vol.9, Issue 1: 13-23, DOI: 10.25236/AJETS.2026.090102

ensuring stable and extensible segmentation, thereby providing a clear and strict spatial constraint framework for the subsequent defect detection pipeline. The line-fitting results are shown in Figure 6.

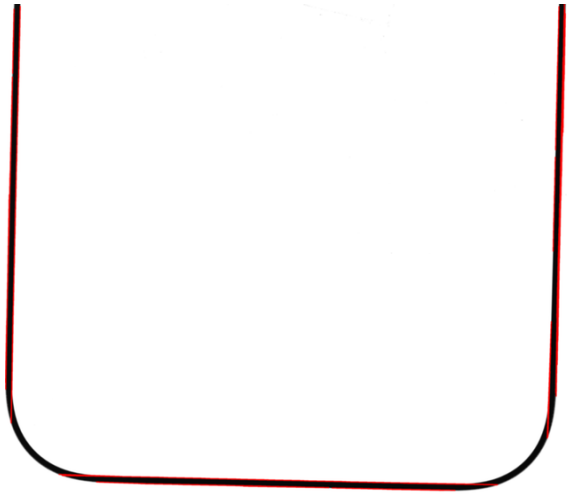

Figure 6: Line Fitting Results.

After obtaining candidate lines using the Hough transform, it is necessary to further screen them according to the placement characteristics of the cover glass on the actual workstation. Since the cover glass is positioned on the workbench by suction nozzles, slight rotational deviations may occur, such that the bottom edge is not perfectly horizontal but exhibits a small tilt angle. Therefore, the line parameters (ρ,θ) produced by the Hough transform are first converted into an explicit representation in the image coordinate system as:

$$y = kx + b \tag{8}$$

The slope k and intercept b can be obtained from the following relationships:

$$k = -\frac{\cos\theta}{\sin\theta}, \quad b = \frac{\rho}{\sin\theta} \tag{9}$$

Based on this representation, the candidate lines can be further screened using joint constraints on both orientation and position. Considering that the cover glass may exhibit a slight rotational deviation when placed by suction nozzles on the production line, an angular constraint is imposed to ensure that the selected line is aligned with the true bottom edge. Specifically, the tilt angle corresponding to the slope k is computed as:

$$\phi = \arctan(k) \tag{10}$$

And filtered by enforcing the following constraint $|\phi| \leq 10^{\circ}$, thereby removing spurious lines with excessively large tilt angles that do not correspond to the true bottom edge.

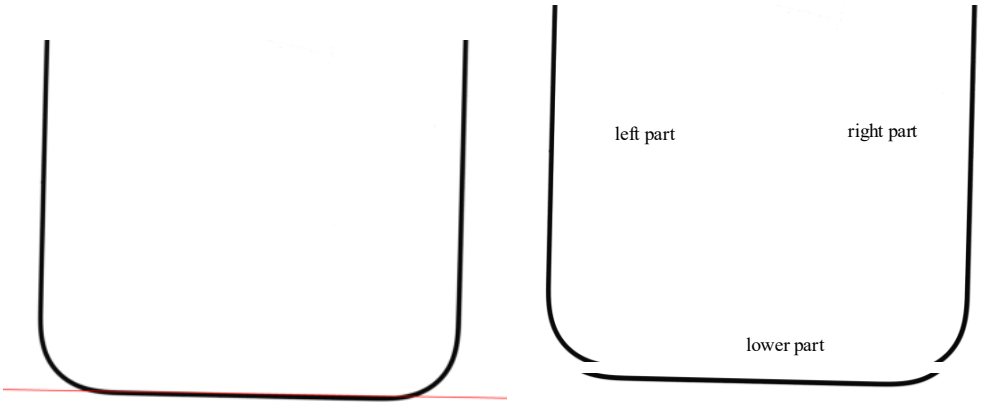

(a) Selected line fitting result after screening *(b) Segmentation result*

Figure 7: Final Results.

ISSN 2616-5767 Vol.9, Issue 1: 13-23, DOI: 10.25236/AJETS.2026.090102

Among the lines that satisfy the angular constraint, a further selection is performed based on the intercept b. Since the bottom screen-printed edge is located in the lower part of the image coordinate system, the corresponding intercept b tends to be larger. Therefore, the line with the maximum intercept, i.e., $b = \max(b_i)$, is chosen as the final segmentation reference. This line provides the best alignment with the inner boundary of the bottom screen-printed edge, enabling stable segmentation of the entire image. The resulting single selected line is shown in Figure 7(a).

2.3 Ink Protrusion Defect Detection

After image segmentation, to achieve stable detection of screen-printed ink protrusion defects, this study proposes a protrusion identification method based on row-wise local response integration and statistical constraints. The proposed method exploits the local structural continuity of the screen-printed edge by constructing a row-level intensity-response model, a ratio-based adaptive threshold, and a structural consistency constraint, thereby enabling accurate localization of low-contrast protrusion defects. The technical workflow is illustrated in Figure 8.

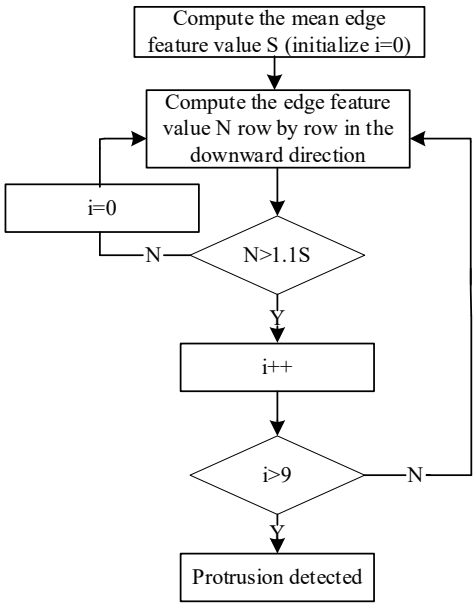

Figure 8: Technical Workflow for Protrusion Detection.

2.3.1 Row-start edge point detection

Taking the left region as an example (with a left-to-right scanning direction), a protrusion typically appears as dark ink pixels that emerge earlier along the scanning direction. Therefore, the first edge point of each row is first determined as follows:

$$x_i^* = \min\{x|\ I(x,i) \neq 255\} \tag{11}$$

where $I(x,i)$ denotes the grayscale value of the enhanced image.

This point can be regarded as the earliest response position of the ink structure along the row direction, and a protrusion causes x_i^* to shift earlier along the scanning direction within a local region.

2.3.2 Local neighborhood response integration

To quantify the ink-structure intensity near the row start, a local neighborhood response integration model is constructed around the row-start region as follows:

$$F_i = \sum_{k=0}^{4}\left(255 - I(x_i^* + k, i)\right) \tag{12}$$

Here, he neighborhood width is set to 5 pixels, according to the typical width of the screen-printed ink edge (approximately 3–6 px); e term (255−I) is used to emphasize the contribution of low-intensity (dark) ink regions, making protrusion-induced structural disturbances more pronounced. F_i represents the local response intensity of the edge in the i row.

ISSN 2616-5767 Vol.9, Issue 1: 13-23, DOI: 10.25236/AJETS.2026.090102

Within the normal screen printing edge area, the distribution of F_i exhibits good consistency between rows, while protrusions cause significantly elevated F_i values.

2.3.3 Ratio-based Adaptive Thresholding Decision Model

To effectively distinguish normal rows from abnormal rows, a ratio-based adaptive thresholding strategy is adopted based on the row-wise mean. First, the mean response of all rows within the region is computed as:

$$\mu = \frac{1}{N}\sum_{i=1}^{N} F_i \tag{13}$$

The i-th row is regarded as a protrusion-candidate row if the following condition is satisfied:

$$F_i > \gamma\mu, \tag{14}$$

Here, γ=1.1 is empirically determined from extensive samples to reflect the pronounced upward shift of the row-level statistics in protrusion regions. Compared with a fixed threshold, this ratio-based threshold can automatically adapt to intensity variations caused by different levels of glass reflection and ink density, thereby improving detection robustness.

Ink protrusions typically manifest as locally continuous structures across adjacent rows, whereas isolated intensity noise or dust particles do not exhibit such continuity. Therefore, a structural consistency constraint is introduced, and consecutive abnormal rows are used as the criterion for determining a protrusion region, as follows:

$$\{i, i+1, \ldots, i+9\} \subseteq \mathcal{A}, \tag{15}$$

Let $A = \{i \mid F_i > \gamma\mu\}$ denote the set of abnormal rows.

The constraint of 10 consecutive rows is motivated by the physical continuity of protrusions (typically corresponding to an edge length of about 0.15 mm). This constraint can effectively suppress false detections caused by isolated noise and significantly improves the reliability of the detection results.

3. Experiment and Analysis

The experimental platform consists of two 20-megapixel industrial cameras and an LED area light source, operating in a backlight imaging configuration. The mobile phone cover glass is placed above the area light source for image acquisition, as shown in Figure 9. This setup provides uniform and stable illumination as well as high-resolution imaging capability, thereby establishing a reliable experimental basis for clear visualization and robust detection of tiny protrusion defects along the screen-printed edge.

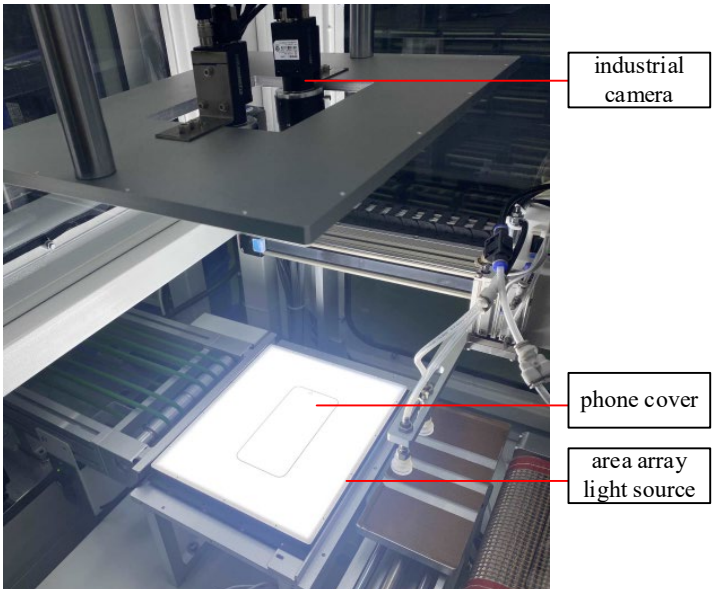

Figure 9: Experimental Platform.

ISSN 2616-5767 Vol.9, Issue 1: 13-23, DOI: 10.25236/AJETS.2026.090102

To further validate the effectiveness and engineering applicability of the proposed method in actual production line scenarios, this paper compares the proposed algorithm with the factory's existing deep learning detection solution. The baseline comparison model selected is the factory's currently deployed YOLOv11n object detection model, which was trained by the factory using historical production line data and is used for online detection. Experimental data also originates from real production samples: 200 qualified cover plates were randomly sampled from the production line and mixed with 100 samples exhibiting ink protrusion defects to construct a unified test set comprising 300 samples in total. All methods underwent offline evaluation on the same test set, with false positives, false negatives, and detection accuracy calculated. Overall results are shown in Table 1, while partial detection visualizations are presented in Figure 10.

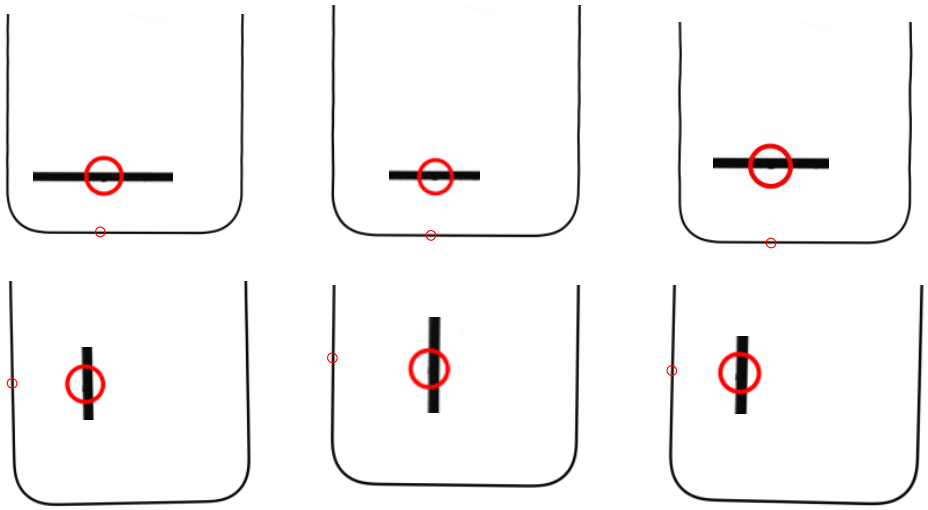

Figure 10: Test results from the methods section of this paper

Table 1 indicates that the factory's YOLOv11n model produced 3 false positives and 21 false negatives on this test set, achieving 92% detection accuracy. In contrast, the proposed method achieved zero false positives and two false negatives on the same 300 test samples, yielding a detection accuracy of 99.33%. These results indicate that for detecting defects like raised screen printing ink—characterized by extremely small scale, weak contrast, and proximity to regular edges—general object detection networks are more susceptible to interference from strong edge structures and texture noise, leading to higher false negative rates. Our approach, however, employs “edge enhancement + geometric baseline constraints + line-scan statistical discrimination” to model defect-prone regions specifically. By introducing continuity constraints to suppress isolated noise, it significantly reduces both false negatives and false positives, demonstrating superior stability and engineering adaptability.

Table 1: Test Results

Method	Sample size	Number of false positives	Number of missed inspections	Detection accuracy rate
Deep learning methods	300	3	21	92.00%
Methodology of This Paper	300	0	2	99.33 %

4. Conclusion

This paper proposes an ink-protrusion defect detection method for mobile phone cover-glass screen-printing scenarios. By integrating image enhancement, Hough line fitting–based image segmentation, and a row-scanning statistical detection strategy, the proposed method addresses challenges such as low contrast, background interference, and the difficulty of recognizing tiny protrusion structures. Experimental results demonstrate that the method achieves high detection accuracy, fast computational speed, and strong robustness, making it suitable for online inspection systems in practical production lines.

ISSN 2616-5767 Vol.9, Issue 1: 13-23, DOI: 10.25236/AJETS.2026.090102

References

[1] Zhu Boyu. Differentiation Breakthrough Strategies for the Current Homogenization of Products in the Mobile Phone Industry [J]. China Collective Economy, 2022, (23): 51-53.
[2] Wu Bayi, Screen Printing Process for Mobile Phone Front Covers. Jiangxi Province, Jiangxi HeliTech Co., Ltd., June 28, 2019.
[3] Liu M J, Zhuang R, Guo X F, et al. Application of improved Otsu threshold segmentation algorithm in mobile phone screen defect detection[C]//2020 Chinese Control And Decision Conference (CCDC). IEEE, 2020: 4919-4924.
[4] Zhang Caixia, Chen Xiaorong, Xu Yunjie, et al. Research on Glass Surface Defect Detection System [J]. Packaging Engineering, 2020, 41(13): 216-222.
[5] Cai Nian, Li Weibo, Huang Qinhao, et al. Defect Detection of Glass-Packaged Insulated Terminals Based on Sector Neighborhood Feature Engineering [J]. Transactions of the Chinese Academy of Electronics and Information Technology, 2022, 44(05): 1548-1553.
[6] Chen Ning, Guo Gangxiang, Guo Bin, et al. Research on Defect Detection Methods for Curved Glass in Mobile Phones [J]. Chinese Journal of Metrology, 2023, 44(05): 701-706.
[7] Ren S, He K, Girshick R, et al. Faster R-CNN: Towards real-time object detection with region proposal networks[J]. IEEE transactions on pattern analysis and machine intelligence, 2016, 39(6): 1137-1149.
[8] Redmon J, Divvala S, Girshick R, et al. You only look once: Unified,real-time object detection[C]//Proceedings of the IEEE conference on computer vision and pattern recognition. 2016: 779-788.
[9] Liu W, Anguelov D, Erhan D, et al. Ssd: Single shot multibox detector [C]// Computer Vision–ECCV 2016. Springer International Publishing, 2016: 21-37.
[10] Yuan Z C, Zhang Z T, Su H, et al. Vision-based defect detection for mobile phone cover glass using deep neural networks[J]. International Journal of Precision Engineering and Manufacturing, 2018, 19: 801-810.
[11] Lv Y, Ma L, Jiang H. A mobile phone screen cover glass defect detection model based on small samples learning[C]//2019 IEEE 4th International Conference on Signal and Image Processing (ICSIP). IEEE, 2019: 1055-1059.
[12] Tomasi C, Manduchi R. Bilateral filtering for gray and color images[C]//Sixth international conference on computer vision (IEEE Cat. No. 98CH36271). IEEE, 1998: 839-846.
[13] Rahmdel P S, Comley R, Shi D, et al. A Review of Hough Transform and Line Segment Detection Approaches[J]. VISAPP (1), 2015: 411-418.
[14] Dharampal V M. Methods of image edge detection: A review[J]. J. Electr. Electron. Syst, 2015, 4(2): 2332-0796.
[15] Gao W, Zhang X, Yang L, et al. An improved Sobel edge detection[C]//2010 3rd International conference on computer science and information technology. IEEE, 2010, 5: 67-71.
[16] Rong W, Li Z, Zhang W, et al. An improved CANNY edge detection algorithm[C]//2014 IEEE international conference on mechatronics and automation. IEEE, 2014: 577-582.
[17] Afshari H H, Gadsden S A, Habibi S. Gaussian filters for parameter and state estimation: A general review of theory and recent trends[J]. Signal Processing, 2017, 135: 218-238.